

Smoke, Sparks, Flames or Explosions? An Experimental Study into how Lithium-ion Cell Failure Varies in Open Field

Katie C. Abbott, Jason Gill, Jonathan E.H. Buston, HSE Science and Research Centre, Buxton, Derbyshire, SK17 9JN

Cells of the same format, size and capacity but differing chemistries can display dramatically different failure mechanisms. A combination of closed and open field testing has been conducted including accelerating rate calorimetry (ARC), downward force, and projectile tests to explore cell behaviour during failure. Four types of failure modes have been identified: (i) smoke and fumes with little to no flame produced; (ii) an aggressive jet flame containing molten metallic particles; (iii) a fireball ejecting the contents of the cell; and (iv) complete rupture and/or fragmentation of the cell. These visually identifiable behaviours lead to further questions about pressures and forces each failure mode generates and therefore the damage they can inflict, the projected flame dimensions and duration of the event, as well as the possibility of spreading fire to additional locations. Numerous incidents have been reported involving lithium-ion batteries, therefore better understanding of these vastly different failure mechanisms is crucial to the development of effective means to mitigate, suppress or prevent the events. Currently, it is not possible to rely on models alone to predict the outcomes of these events due to there being too many factors at play. In addition, many of the specific conditions are unknown or not evident, especially when closed cell testing techniques such as ARC are used in isolation. The work presented here offers experimental results and a practical perspective on cell behaviour during failure in open field testing that informs better understanding of this technology. Different failure modes have been demonstrated between three different cells, but also within the same type of cell.

Keywords: Thermal runaway, lithium-ion battery, thermal hazards, accelerating rate calorimetry (ARC), battery fire, battery explosion, projectiles

Introduction

Lithium-ion batteries (LIBs) form an essential component of transportation and energy storage as part of the global drive to Net Zero. They are increasingly being used across numerous applications in many different formats. Batteries store energy in chemical form, and the majority of LIB cells use a flammable electrolyte. When a cell fails, its stored energy can be released, and the components can combust in several ways resulting in heat and gas release, fire and explosions (Garche Jurgen, Brandt Klaus, 2019).

Cell failure occurs when the heat generated overcomes the heat dissipated, and the cell enters an uncontrolled state of increasing temperature until failure occurs, a term known as thermal runaway (TR) (Q. Wang et al., 2019). This can happen when a cell is exposed to abnormal operating or external conditions, such as excessive temperatures or impact. Research has been carried out to investigate the mechanisms behind TR, but the diversity of cell chemistries adds an increased level of complexity (Wang et al., 2020b)(Golubkov et al., 2014)(Feng et al., 2019a). Extensive research has been previously conducted to explore abuse methods to induce cell failure, and these methods can be divided into three categories; mechanical, electrical and thermal (Lopez et al., 2015) (Karp, 2019) (Wang et al., 2020a).

Accelerating rate calorimetry (ARC) is often used to characterise the TR features of a cell through thermal abuse. ARC tests are often performed to assess the thermal stability of LIBs (Feng et al., 2019a) (Lei et al., 2017) (Brand et al., 2013). Tests are carried out under adiabatic conditions, to determine the onset temperature of the reaction. This method achieves the conditions to mimic the worst-case scenario for a cell, but does not allow visualisation of the way in which they fail. This paper aims to provide a comparative experimental perspective on the failure behaviour of LIBs by performing both closed and open field thermal abuse tests.

TR is a generic term to describe the failure of cells; however individual cells can behave differently during TR. A recent study investigating the potential thermal hazards of LIBs identified sparks and jet fire events during final failure (Chen et al., 2020). Cell rupture and tearing during failure has also been observed in multiple studies (Said et al., 2019) (Lao et al., 2020) (Said et al., 2020). These varied types of failure modes have the potential to cause serious harm to bystanders, with the potential to propagate to neighbouring cells and escalate to large scale fires (Said et al., 2019). However, there is currently no definitive advice on assessment of the subsequent damage and hazards a cell failing can inflict. With studies revealing alternate failure modes, questions arise regarding specific cell behaviour during failure and how this affects the fire risk posed by the cells.

The hazards associated with a battery can also vary with state of charge (SoC), cell chemistry and size. Lower SoC cells are seen as safer due to the reduced energy contained, compared to higher SoC which have an increased stored energy and can achieve higher temperatures (Z. Wang et al., 2019). Baird et al. (2020) conducted a study to identify the explosion hazards of battery vent gases, and found that they differ with cathode material. Cathode material also affects the type of failure in cell arrays, and the types and quantities of gases emitted during TR which introduce toxicity concerns (Said et al., 2020). This study looks at high capacity (nominally 5 Ah) 21700 (21 mm diameter and 70 mm height) hard case cylindrical cells at 100% SoC to access the failure modes and potential differences between electrically similar commercial cells.

Methodology

Cells Tested

Abuse tests were performed on three types of 21700 cylindrical LIBs designated, 1, 2 and 3. The specification for each cell type can be found in Table 1. The cells were charged to 100 % according to the manufacturer's instructions. 100 % SoC cells were used as this charge has the highest energy and therefore has the potential to cause the most damage (Z. Wang et al., 2019), thus worst case. These three cells have similar capacities but are from a variety of manufacturers.

Table 1 Cell manufacturer's specification for cells 1, 2 and 3

	Cell 1	Cell 2	Cell 3
Nominal Capacity	5.0 Ah	4.9 Ah	4.7 Ah
Nominal Voltage	3.63 V	3.63 V	3.64 V
Weight	≈ 63 g	≈ 67 g	≈ 67 g

ARC

Cells at 100 % SoC were heated in an adiabatic environment in an ARC-EV (THT) using the typical heat-wait-seek algorithm. The test sample was placed inside a blast box within the ARC. The initial temperature was determined (50 °C in this case), and the battery was then heated at increments of 5 °C. Wait and seek periods continued until self-heating was detected and therefore an exothermic reaction had been achieved. A type-N thermocouple was placed along the centre of the cell and recorded the cells surface temperature during the test.

One test per cell was conducted to determine at what temperature the internal self-heating process that eventually leads to thermal runaway begins, providing accurate data when all external variables are controlled. These results represent the worst-case scenario where self-sustaining thermal runaway is truly achieved, characterised by some key parameters referred to in literature studies (Feng et al., 2019b) (Feng et al., 2019a):

- T_1 is the self-heat onset temperature and is defined as the point where self-heating is detected.
- T_2 is the temperature when the cell began to vent, indicated by a sudden decrease in temperature.
- T_3 is the maximum observed temperature during TR.

Downward Force Measurements

Testing *via* external heating was carried out on a load cell to try to understand the downward forces generated when a cell undergoes catastrophic failure. All testing was carried out within a bespoke testing facility. The three types of cells were externally heated, using an adhesive 2" x 2" heating pad with 30 W applied, until thermal runaway was achieved, and data was collected. The cells were positioned on top of a 5 kg load cell (Figure 1), and the cells surface temperature was measured using a type-K thermocouple. Impulse is the integral of the force, calculated from the load cell voltage output measurements, over the time interval for which it acts. It was calculated using Simpson's rule.

$$\int_a^b P(x)dx \approx \frac{h}{3}[f(a) + 4f\left(\frac{a+b}{2}\right) + f(b)] \quad (1)$$

Where:

- h is the interval of the data collection.
- a is the lower integral limit, in this case, the start time for TR.
- b is the upper integral limit, in this case, the end time for TR.

High speed video footage was also analysed to visually characterise the failure modes across the three cell types

Figure 1 The 5 kg load cell set up

Projectiles – Cell Heated by Flame

Finally, projectile testing was conducted on the three types of cells to understand the cells trajectory during failure, and the potential consequential damage to surrounding areas. Two heating methods were used to induce cell failure. The first method used a Bunsen burner to heat each cell. Cells were held inside a capped metal tube (positive terminal inserted first) attached to a clamp stand, and the Bunsen burner was situated below the cell to be tested. Two high speed cameras were used to capture the event, a wide camera capturing images at 1000 fps (frames per second), and a close-up camera at 10,000 fps 3 m away from the cell. The close-up camera was used to calculate the initial average speed of the cell. The overall length of the test pad was 11 m, and the Bunsen burner was 50 mm below the cell. Protection from cells/cell fragments was provided by a 0.5 m thick concrete block wall.

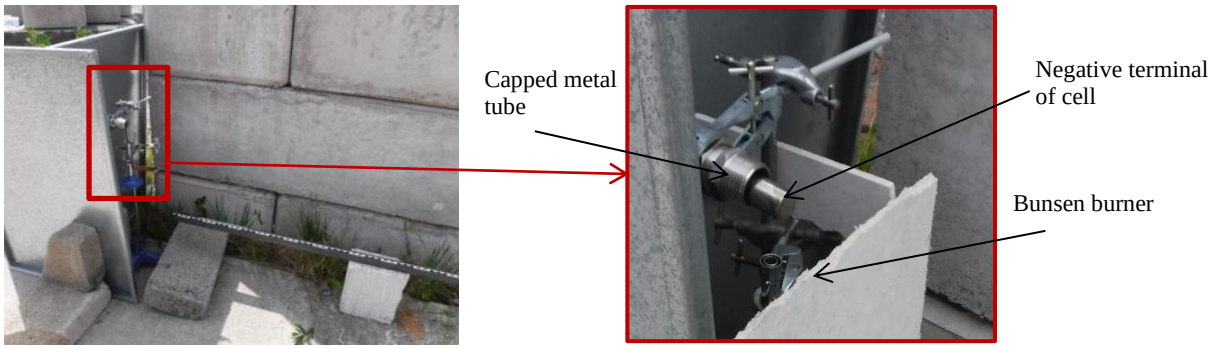

Figure 2 The projectile test set up and test pad using a Bunsen Burner

Projectiles – Cell Heated by Radiant Heater

The second heating method used an adhesive 3” x 2” heating pad, with 60 W applied. The cell was held inside an insulated copper capped tube which was heated. The tube was clamped to a bespoke test rig and the cell was placed positive terminal first inside the tube. The test pad was circular and had a circumference of 30 m. A high-speed camera at 10,000 fps was situated 3 m away from the cell, and a further camera at 120 fps was used to capture the entire trajectory of the cell. The high speed camera was used to calculate the initial average speed of the cell. Protection from cells/cell fragments was provided by a 0.5 m thick concrete block wall.

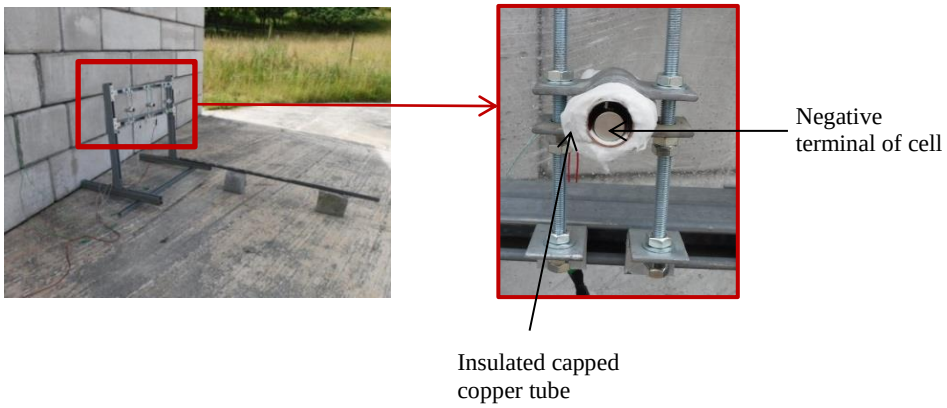

Figure 3 The projectile test set up and test pad using an electric heater

Results

ARC

Cell temperature as a function of time for single tests are shown in Figure 4, with the key parameters summarised in Table 2. A similar trend can be observed with comparable self-heating onset and maximum temperatures. The only noticeable difference is the decreased time it takes for cell 1 to enter thermal runaway.

The self-heating onset temperature (T_1) for cell 2 was detected at a lower temperature (~84 °C) compared to cell 1 (~87 °C) and cell 3 (~92 °C). This lower temperature indicates a decreased safety region compared to cells 1 and 3, with cell 3 remaining stable to the highest temperature. Cell type 1 vented (T_2) at a lower temperature (~116 °C) compared to cell 2 (~130 °C) and cell 3 (~127 °C). The maximum temperatures recorded are very low in all three cell types, and were expected to reach temperatures in excess of 500 °C (Feng et al., 2019b). However, cell types 2 and 3 ejected their jelly roll (Figure 5); therefore the thermocouple was measuring the empty can, and the thermocouple was displaced during the cell type 1 test. This explains why the temperature drops very rapidly in Figure 4.

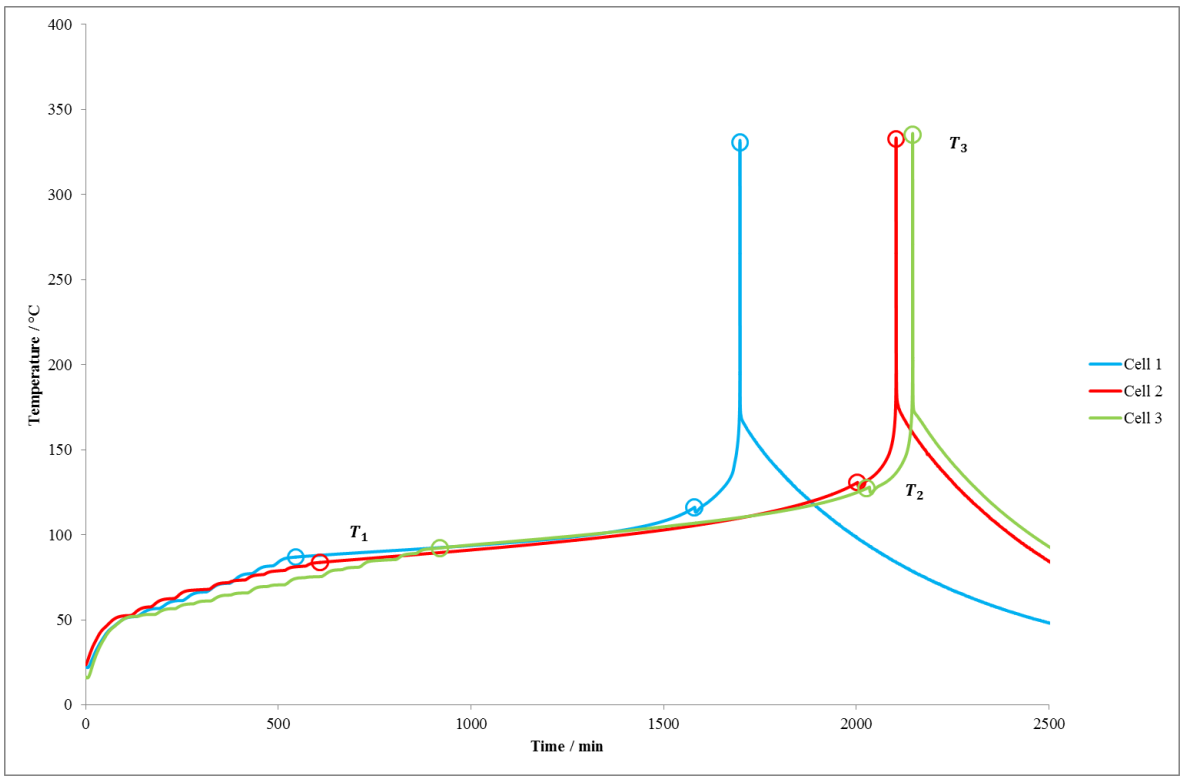

Figure 4 Temperatures as a function of time for cells 1, 2 and 3

Table 2: Summary of the ARC Test Results

Cell Type	SoC	T_1 Self-heat onset Temperature (°C)	T_2 Temperature at Initial Vent (°C)	T_3 Maximum Observed TR Temperature (°C)
1	100	87	116	331
2	100	84	130	333
3	100	92	127	335

Figure 5 Post-test photos of cell type 1, 2 and 3 (from left-right)

Downward Force Measurements

Downward force tests were repeated three times per cell type. Tests conducted on type 1 cells resulted in very similar visual observations during failure. The general failure included cell venting with the production of smoke and gases, sparking, and then a flame was produced which engulfed the cell (Figure 6). This failure event took around 20-30 seconds, with the main flame event lasting ≤5 seconds. The final part of the flame was the heater burning. All three type 1 cells only partially ejected their contents.

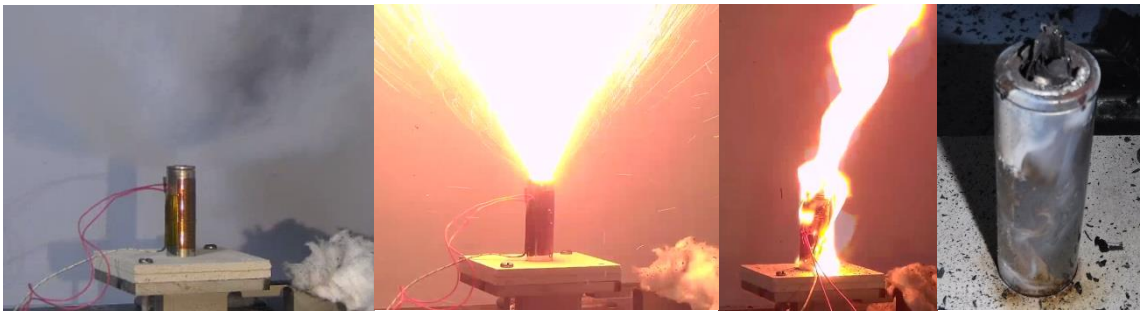

Figure 6 Evolution of cell type 1 failure including venting, sparking and a flame engulfing the cell, and the cell after the test (from left-right)

Two types of failure modes were observed within the three tests for cell type 2 (Figure 7). The first failure event resulted in a fireball and complete rupture of the cell, with the cell being split into two pieces. The cell contents were ejected and remained on fire in the blast chamber for a short while. The second type of failure mode observed also included the cell projecting a fireball upwards and then returning to a steady flame, however there was no noticeable damage to the cell casing. The entire cell cap was removed during cell failure with its entire contents emptied. The high speed footage revealed an explosive and violent event for cell type 2 failures, with very noticeable recoil of the cell holder. Both failure events took around 60-80 seconds, with the main fireball event lasting typically ≤3 seconds.

Figure 7 The projected fireballs captured on the high speed camera during cell type 2 failure, showing the cell being split in two and the after photo (left) and another typical projected fireball and the after photo (right)

The failure mode for cell type 3 resulted in ejection of the cells contents and the doming of the bottom of the cell. The flame produced can be described as an aggressive jet flame followed by the ejection of molten metallic particles (Figure 8). The failure event took around 60-80 seconds, with the aggressive flame event lasting typically ≤3 seconds.

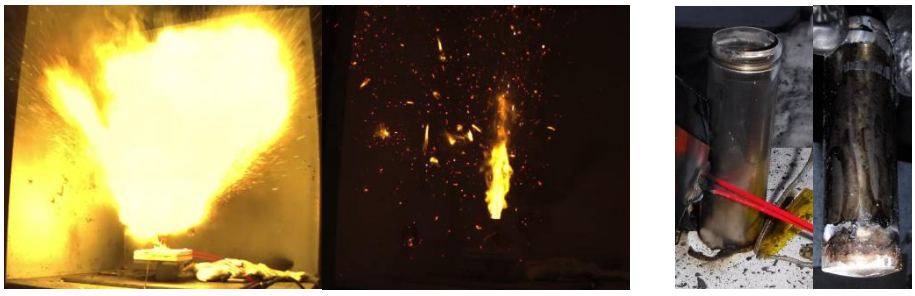

Figure 8 The aggressive jet flame captured on the high speed camera during cell type 3 failure and the ejection of molten metallic particles (left), and the cell after the test (right)

Table 3 Downward force data from repeat tests on cells 1, 2 and 3

Cell Type	Test	SoC	Mass Loss (%)	Maximum Recorded Temperature (°C)	Final Failure Onset Temperature (°C)	Maximum Downwards Pressure (kPa)	Impulse (kPa.s^{-1})	Duration of Event (s)
1	1	100	74	554	193	17.2	8.2	1.20
1	2	100	80	702	202	57.5	9.4	1.00
1	3	100	75	703	196	67.1	12.9	0.40
2	4	100	86	176	176	7.3	0.7	0.20
2	5	100	-	608	185	14.5	1.6	0.23
2	6	100	80	484	189	14.7	1.6	0.28
3	7	100	47	397	235	6.6	0.71	0.22
3	8	100	81	481	174	20.7	2.3	0.26
3	9	100	80	-	-	10.8	1.2	0.22

Note that temperature data is not included for test 9 as the thermocouple detached from the cell early in the test. Test 4 was where cell type 2 ruptured and split into two pieces. The rupture detached the thermocouple at the point of failure, hence this was the maximum temperature recorded. Mass was not recorded in test 5.

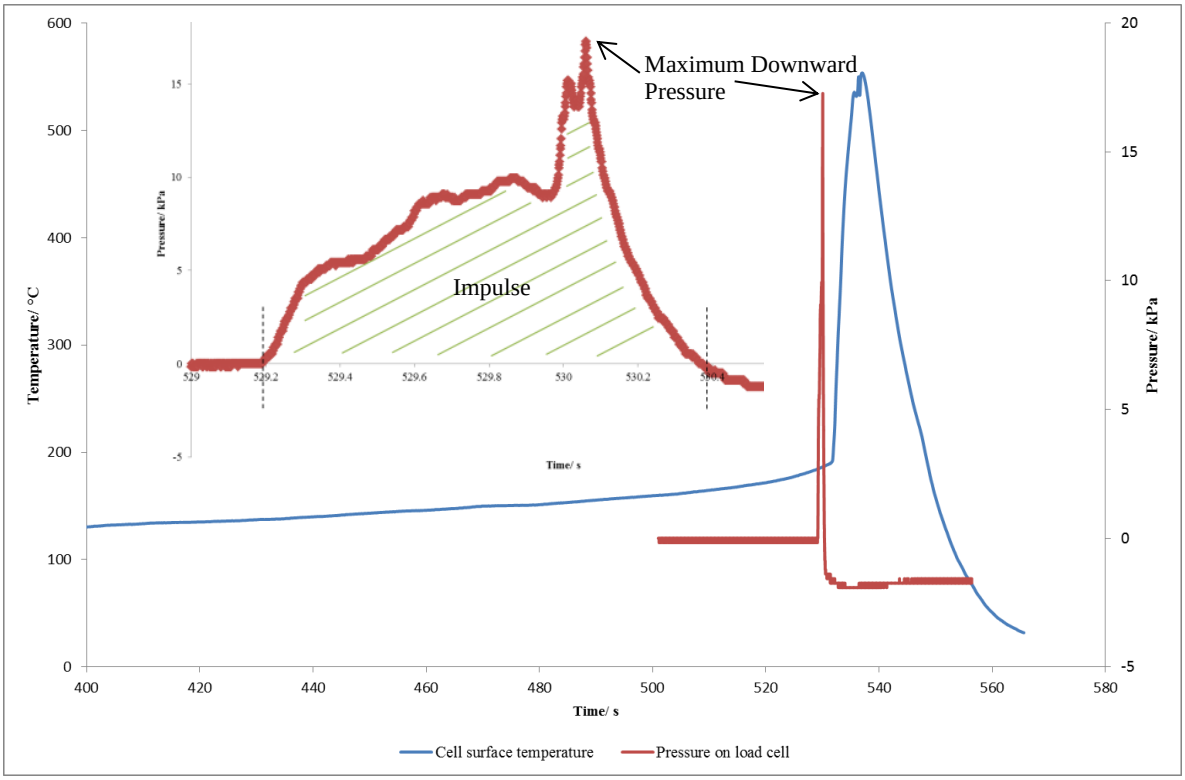

Figure 9 A sample graph of temperature and pressure as a function of time for test 1, with a close up of the pressure graph used to calculate impulse

Cell type 1 reached the highest maximum temperature during cell failure (703 °C) and the highest maximum pressure (67.1 kPa). This however didn't yield a significant increase in impulse due to its short duration. As a result, impulse could be perceived as a better measurement to compare cells as it takes into account the duration of the event. With that in mind, cell type 1 produced the highest impulse measurement compared to the other cells (12.9 kPa.s^{-1}). This can be explained by the type of failure mechanism observed. For cell type 1 the contents remained in situ within the cell for longer, burning within the can and therefore producing a higher impulse. Cell type 2 and 3 both ejected their contents, resulting in a violent failure event that happened elsewhere and therefore wasn't recorded on the load cell. This early ejection of contents also resulted in lower maximum temperatures for cell types 2 and 3.

Projectiles – Cell Heated by Flame

The average speed for each cell type was analysed using the Phantom Camera Control (PCC) software provided by the camera manufacturer and are shown in Table 4. It should be noted that this software only provides an indication of the speed, as it was only designed to track object movement in the plane of view. It does however provide a clear indication of the speeds generated when a cell projects during TR and offers a way to compare the failure modes of different cells. A repeat of cell type 3 was conducted as the first test resulted in the cell projecting in an upwards trajectory, meaning the speed was difficult to calculate reliably. Cell type 2 had the highest average speed when travelling 2 m (23 ms^{-1}), followed by cell type 1 (14 ms^{-1}), then cell type 3 (4 & 11 ms^{-1}).

Table 4 Speed data analysed using the Phantom Camera Software. These speeds were based on a camera view of approximately 2 m. The cells travelled further than this.

Cell Type	Average Speed (ms^{-1})
1	14
2	23
3	4
3	11

Different failure modes were observed when analysing the high speed camera footage after the test and are displayed in Figure 10. The approximate trajectories are shown in Figure 11. Sparks were seen ejecting out of the top and bottom of cell 1, as shown in Figure 10A, causing the cell to spin whilst travelling in a fairly straight trajectory (Figure 11A). It landed on the floor before impacting the wall of the test pad, meaning that it couldn't have travelled much further than 11 m. Analysis of the cell after the test revealed a small rupture hole in the bottom where the sparks were released from. This corresponded to the area of the cell where the flame was applied. The cells contents were not ejected.

Cell 2 on the other hand demonstrated a different failure mode. The cell vented flame only from the positive terminal end and travelled without spinning. The cell then appeared to rupture with the case following an upward trajectory out of the test arena (Figure 11B). The majority of the jelly roll contents of the cell were observed to follow a horizontal trajectory, before impacting the wall and coming to a stop on fire. The only remains of the cell that could be found after the test were remnants of its contents, which were deposited through impact on the test pad wall. The remaining parts of the cell travelled out of the test arena and could not be located.

The first test using cell 3 resulted in an upwards projection of the cell. The cell started to travel towards the ground after producing an aggressive jet flame, but then changed its path and accelerated towards the sky whilst spinning. Large amounts of sparks, smoke / fume were produced during the event; see Figure 10C, with sparks only coming from the positive end of the cell. The repeated test of cell 3 resulted in a different failure response. Parts of the cell fragmented upon release producing smoke and a lot of sparks as shown in Figure 10D. This cell followed a fairly straight trajectory before striking the test pad wall. It would be expected that this cell would have travelled much further than 11 m had the wall not stopped it.

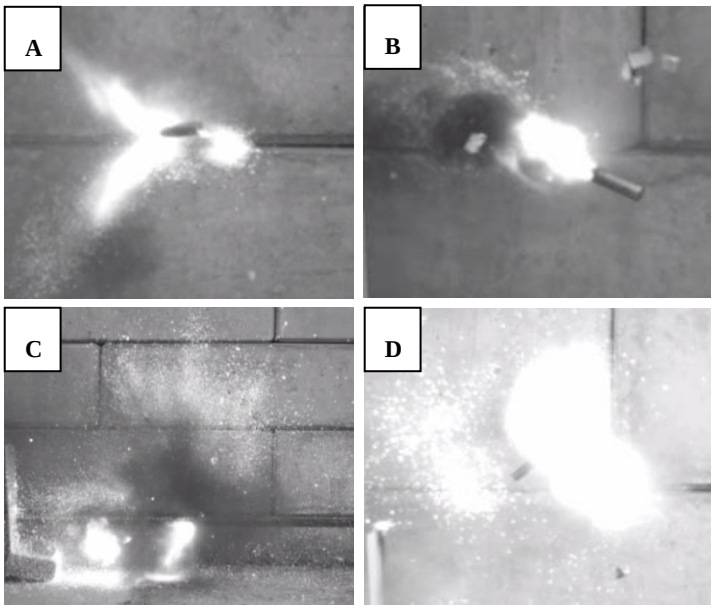

Figure 10 Screenshots from the high speed footage indicating the failure of cell type 1 (A), type 2 (B) and type 3 (C &D)

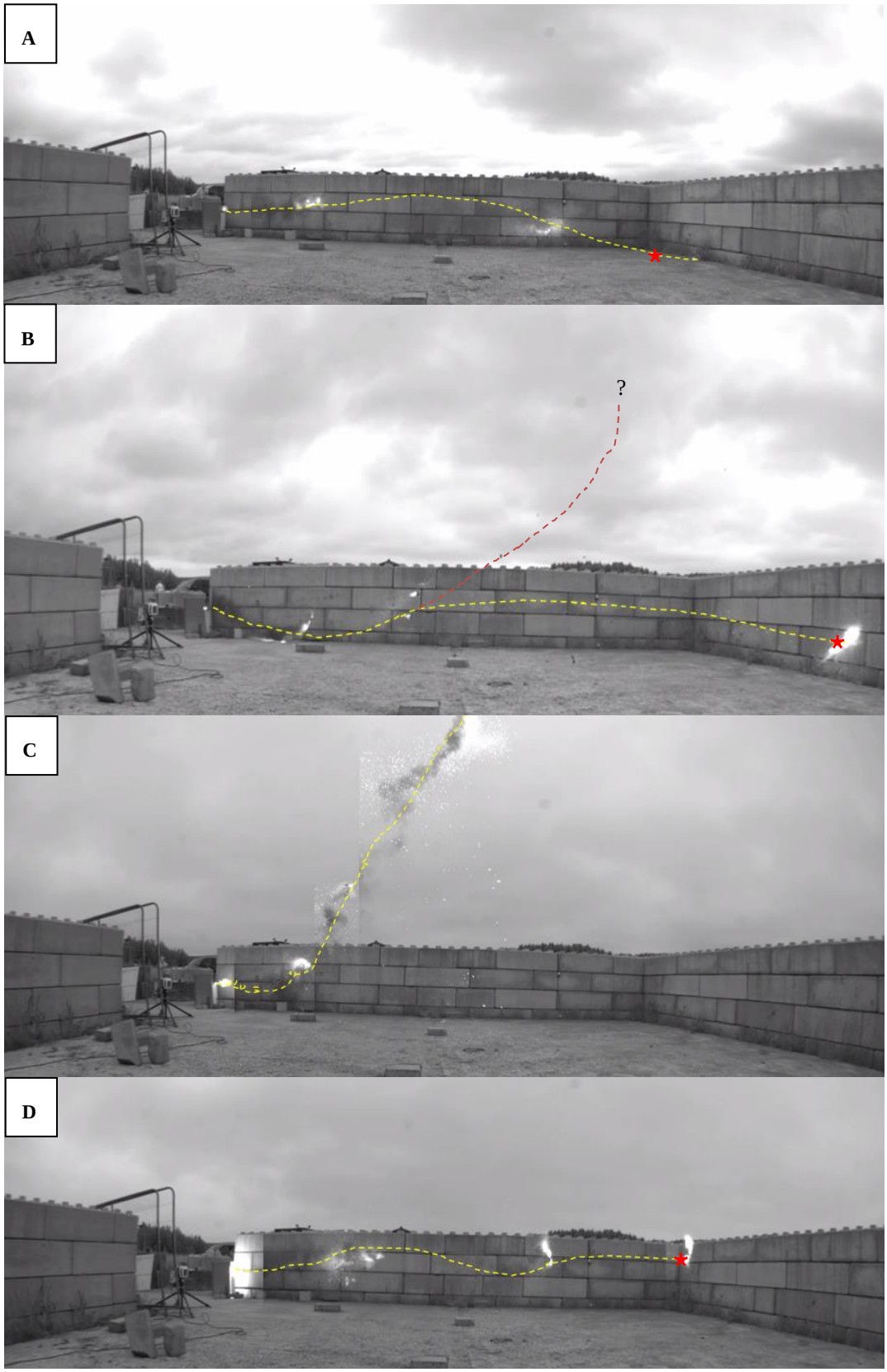

Figure 11 An overlay of screenshots from the wide view high speed camera to show trajectories for cell type 1 (A), cell type 2 (B) and cell type 3 (C &D). The red star indicates where the cell impacted the floor / wall

Projectiles – Cell Heated by Radiant Heater

The same method as described in the above section was used to analyse the average speed of the cells using the PCC software. Cell type 2 had the highest average speed when travelling 1.5 m (62 $m.s^{-1}$), followed by cell 3 (60 $m.s^{-1}$), and then cell 1 (13 $m.s^{-1}$). Cell type 2 travelled the furthest distance (37 m), followed by cell type 3 (32 m), and then cell type 1 (26 m). The estimated landing positions are shown in Figure 12.

Table 5 Speed data calculated using the Phantom Camera Software. These speeds were based on a camera view of approximately 1.5 m. The cells travelled further than this.

Cell Type	Average Speed (ms^{-1})	Total Distance Travelled (m)
1	13	26
2	62	37
3	60	32

Cell type 1 ejected its contents during its trajectory, and curved to the right. Camera footage of the entire event showed that the cell was not on fire when it landed. Cell type 2 travelled the furthest, following a fairly straight trajectory (Figure 12). The force with which the cell ejected from the holder caused the copper tube to fall out of the clamp, with the contents of the cell being ejected immediately, landing on fire on the test pad. Cell type 3 also followed a fairly straight trajectory. The force exerted from cell type 3 pushed the copper tube backwards and the cell contents were left in its place on fire - only the empty casing was projected. All cells ejected their contents using this test method, but no rupture or melting holes were observed.

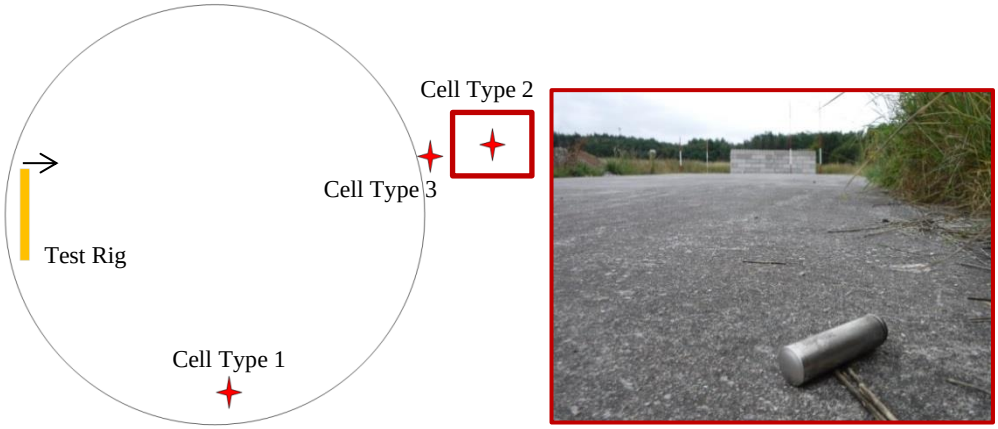

Figure 12 A schematic of where each cell type landed on the test pad (left) and a picture looking back at the test rig from the perspective of cell type 2 (right)

Figure 13 Screenshots from the high speed camera showing the initial projection of cells 1 (left), 2 (middle) and 3 (right)

Discussion

The results obtained from ARC tests indicated that the three cell types tested failed in similar ways. This is explained by the comparable self-heating and final failure onset temperatures recorded which can be used to assess the thermal stability of a cell. Based on this information alone, these cells could be used interchangeably due to their perceived similar failure behaviours. However, open field testing exposed numerous failure mechanisms which cannot be identified through closed testing methods. The maximum temperature a cell reaches will have an impact on the safety design of a battery pack. Any increase in maximum cell temperature will lead to an increased temperature gradient between adjacent cells and thus an increased risk of inducing propagation (Feng et al., 2019a). The comparable maximum temperatures observed during closed testing indicate that no cell type will be at any greater risk of causing propagation compared to another. However, the open field experiments conducted disagree. Post-test video analysis showed that cell type 1 was the only cell that did not eject its contents during downward force and flame heated projectile tests.

Comparing the results from the downward force and projectile testing using a flame for cell type 1, similar failure modes were observed which can be described as the production of smoke, sparks and fumes with little to no flame. The consistent final failure onset temperatures from the load cell tests can also be explained by the comparable failure modes witnessed. The cell did not rupture in any of the open field tests, and had the highest maximum temperature recorded. This higher temperature was likely achieved because this cell type did not eject its contents, retaining more of its mass to burn inside the cell. Consequently, this type of cell has an increased likelihood to cause propagation by heat transfer to neighbouring cells inducing further failures with the potential to cause large scale battery fires (Said et al., 2019).

Complete rupture and fragmentation of the cell was witnessed for cell type 2 in both the downward force and projectile flame tests, with a fireball also observed during the downward force testing. With the contents of the cell ejected, mass was reduced to the cell casing and residues and therefore heat was not retained to the same extent as cell type 1, reducing its likelihood of causing propagation to neighbouring cells. However, as witnessed in the projectile tests, any contents that are ejected are likely to be on fire. The final resting place of these burning contents needs to be managed to prevent propagation via this type of event. A study analysing the possibility of cell rupture during TR also found that the maximum temperature of a ruptured sample was lower than a non-ruptured sample. It was also found that cell rupture was a less common failure response, this uncertainty stemming from the complicated electrochemical reactions that take place within a cell (Lao et al., 2020). The ejected contents travelling at high speed have the potential to cause a secondary fire, and even injury to bystanders. Some reporting suggests that vape battery explosions have resulted in numerous incidents where injuries such as burns and broken bones have been observed (“Vape Danger”, 2019). The projection of cells has also been witnessed during an incident involving a high speed crash of an electric vehicle. The cells damaged by impact projected themselves into nearby residence (Hruska, 2020). These examples highlight the importance of the continuation in the study of failure mechanisms during TR.

Varied failure modes were observed for cell type 3 during open field testing, which included aggressive jet flames and ejected cell contents. The variability in speed, direction and impulse adds an unpredictable characteristic to this cell. This uncertainty in cell behaviour makes it difficult to predict how these cells will respond in any failure event, making choice of hazard mitigation difficult.

When comparing heating methods for projectile testing, different failure modes were identified, with cell types 1 and 2 only rupturing when subject to a flame. Subject to abuse, LIBs will experience an internal short circuit due to the collapse of the separator (Wang et al., 2020a). It has been suggested that cell rupture and tearing is caused by this internal short circuit (Lao et al., 2020). However, the flame may potentially promote localised heating, weakening the shell and increasing the likelihood of rupture. The typical shell material of a LIB is nickel plated cold rolled steel (Wang et al., 2018). Temperatures in excess of 400 °C were recorded during the load cell tests, and it is at this point where steel can begin to soften and undergo a process known as recrystallisation. Recrystallisation is accompanied by a reduction in strength, due to the reduced number of dislocations from the new larger grains formed (Xu and Ferry, 2010). Therefore, this localised method of heating could promote cell rupture and melting holes due to these metallurgical changes. It should be noted that Lao et al (2020) used a localised heating method in their study. Electric heating over a large surface area of the cell provided a more uniform way of heating the cell, reducing the chance of producing localised heating spots. This method caused all cell types tested to eject their entire contents and travel at increased speeds in the projectile tests.

A study on modules also reports that propagation is more likely to occur when a melted hole or tearing crack is observed (Lao et al., 2020). Melted holes were observed during some of the flame heated projectile tests, with holes appearing at both ends for cell type 1. This resulted in venting from both ends, causes a spinning motion during the trajectory (Figure 8a). This type of failure potentially reduces the possibility of losing its contents, and therefore increases the chance of projectiles landing at increased temperatures, potentially initiating further events. This highlights the importance of the investigation into the mechanisms behind cell rupture and other non-standard failure mechanisms.

Different failure modes have been demonstrated between the three cell types tested, but also within the same type of cell. The forces exerted and the speed and distance of the ejected cells has the potential to penetrate and damage surrounding areas, including the integrity of a pack of cells. The nature of these projectiles is also highly dangerous to any member of the public that might be nearby. The violent rupture of some cells along with the ejection of burning cell contents raise concerns for the safety of the public and first responders due to a threat of radiative heat or projected fire, or hot objects with sufficient mass to cause damage. Standoff distances are not well studied, which is understandable, given the variability we see during cell failure, an increase in knowledge and awareness in this area is needed.

Conclusion

Multiple failure modes for cells of the same size and electrical properties, but from different manufactures have been identified through a combination of closed and open field testing. The comparable ARC results for the three types of cells allude that the cells fail in similar ways, however the visual observations identified through open field testing disagrees. One cell type generally stayed intact, with the other two ejecting their contents during failure. The cell type and failure modes equate to differing hazards in cases of potential cell failure propagation through a pack, projectile, and fire spread risk. It will also affect the way any incidents involving these types of cells are managed. The reported experimental results indicate a need for a greater awareness of the different failure modes that can occur which can in turn affect battery selection, transportation and storage applications. With the rapid growth of LIBs, open field testing is needed to continually assess the behaviour of cells, new and old, to help identify ways to supress, mitigate and stop potential failure events and their consequences. In addition, further research into the distances travelled by failing cells needs to be conducted to provide support to and ensure the safety of first responders. Additional research also needs to be conducted to explore how different heating methods can affect failure mechanisms. Flame heated projectile testing caused a slow moving flaming projectile, compared to the violent ejection of contents during a more uniform method of electric heating, with both of these types of projectiles capable of traveling long distances. This is critical knowledge for those conducting battery safety testing and raises additional questions regarding the damage projected cells and their contents can cause to people and materials.

Acknowledgements and Disclaimer

The work is conducted within the frame of the “Lithium-Ion Battery Research In Safety (LIBRIS)” project funded by Innovate UK.

The work described in this paper were undertaken at the Health and Safety Executive (HSE) Science and Research Centre. Its contents, including any opinions and/or conclusions expressed, are those of the authors alone and do not necessarily reflect HSE policy.

References

Brand, M., Gläser, S., Geder, J., Menacher, S., Obpacher, S., Jossen, A., Quinger, D., 2013. Electrical safety of commercial Li-ion cells based on NMC and NCA technology compared to LFP technology. *World Electr. Veh. J.* 6: 572–580.

Chen, H., Buston, J.E.H., Gill, J., Howard, D., Williams, R.C.E., Rao Vendra, C.M., Shelke, A., Wen, J.X., 2020. An experimental study on thermal runaway characteristics of lithium-ion batteries with high specific energy and prediction of heat release rate. *J. Power Sources* 472: 228585.

Feng, X., Zheng, S., Ren, D., He, X., Wang, L., Cui, H., Liu, X., Jin, C., Zhang, F., Xu, C., Hsu, H., Gao, S., Chen, T., Li, Y., Wang, T., Wang, H., Li, M., Ouyang, M., 2019a. Investigating the thermal runaway mechanisms of lithium-ion batteries based on thermal analysis database. *Appl. Energy* 246: 53–64.

Feng, X., Zheng, S., Ren, D., He, X., Wang, L., Liu, X., Li, M., Ouyang, M., 2019b. Key characteristics for thermal runaway of Li-ion batteries. *Energy Procedia* 158: 4684–4689.

Garche Jurgen, Brandt Klaus, 2019. Li-Battery Safety, in: Garche Jurgen, B.K. (Ed.), *Li-Battery Safety*. pp. 145–165.

Golubkov, A.W., Fuchs, D., Wagner, J., Wiltsche, H., Stangl, C., Fauler, G., Voitic, G., Thaler, A., Hacker, V., 2014. Thermal-runaway experiments on consumer Li-ion batteries with metal-oxide and olivin-type cathodes. *RSC Adv.* 4: 3633–3642.

Hruska, J., 2020. ExtremeTech [WWW Document]. Tesla Model 3 Crash Hurl. Batter. Cells Into Nearby Home. URL https://www.extremetech.com/extreme/317620-tesla-model-3-crash-hurls-battery-cells-into-nearby-home (accessed 8.17.21).

Karp, M., 2019. Thermal Runaway Initiation Methods for Lithium Batteries.

Lao, L., Su, Y., Zhang, Q., Wu, S., 2020. Thermal Runaway Induced Casing Rupture: Formation Mechanism and Effect on Propagation in Cylindrical Lithium Ion Battery Module. J. Electrochem. Soc. 167: 090519.

Lei, B., Zhao, W., Ziebert, C., Uhlmann, N., Rohde, M., Seifert, H.J., 2017. Experimental analysis of thermal runaway in 18650 cylindrical Li-Ion cells using an accelerating rate calorimeter. *Batteries* 3: 1–14.

Lopez, C.F., Jeevarajan, J.A., Mukherjee, P.P., 2015. Experimental analysis of thermal runaway and propagation in lithium-ion battery modules. *J. Electrochem. Soc.* 162: A1905–A1915.

Said, A.O., Lee, C., Stoliarov, S.I., 2020. Experimental investigation of cascading failure in 18650 lithium ion cell arrays: Impact of cathode chemistry. *J. Power Sources* 446: 227347.

Said, A.O., Lee, C., Stoliarov, S.I., Marshall, A.W., 2019. Comprehensive analysis of dynamics and hazards associated with cascading failure in 18650 lithium ion cell arrays. *Appl. Energy* 248 : 415–428.

Vape Danger [WWW Document], 2019. . Vape Batter. Explos. URL https://www.vapedanger.com/vaping/battery-explosion/ (accessed 8.17.21).

Wang, H., Du, Z., Liu, L., Zhang, Z., Hao, J., Wang, Q., Wang, S., 2020a. Study on the Thermal Runaway and Its Propagation of Lithium-Ion Batteries Under Low Pressure. *Fire Technol.*

Wang, H., Du, Z., Rui, X., Wang, S., Jin, C., He, L., Zhang, F., Wang, Q., Feng, X., 2020b. A comparative analysis on thermal runaway behavior of Li (NixCoyMnz) O2 battery with different nickel contents at cell and module level. *J. Hazard. Mater*. 393.

Wang, L., Yin, S., Yu, Z., Wang, Y., Yu, T.X., Zhao, J., Xie, Z., Li, Y., Xu, J., 2018. Unlocking the significant role of shell material for lithium-ion battery safety. *Mater. Des.* 160: 601–610.

Wang, Q., Mao, B., Stoliarov, S.I., Sun, J., 2019. A review of lithium ion battery failure mechanisms and fire prevention strategies. *Prog. Energy Combust. Sci*. 73: 95–131.

Wang, Z., Ouyang, D., Chen, M., Wang, X., Zhang, Z., Wang, J., 2019. Fire behavior of lithium-ion battery with different states of charge induced by high incident heat fluxes. *J. Therm. Anal. Calorim.* 136: 2239–2247.

Xu, W., Ferry, M., 2010. Recrystallisation processes in cold rolled low carbon steel strip containing different starting microstructures. *Mater. Sci. Technol.* 26: 333–342.